Published in final edited form as:
J Comp Neurol. 2014 April 1; 522(5): 986–1003. doi:10.1002/cne.23456.

Expression of m1-type muscarinic acetylcholine receptors by parvalbumin-immunoreactive neurons in the primary visual cortex: a comparative study of rat, guinea pig, ferret, macaque and human

Anita A. Disney[1] and **John H. Reynolds**[1]
[1]Systems Neurobiology Laboratories, The Salk Institute for Biological Studies, La Jolla, California

Keywords

striate cortex; neuromodulation; quantitative; anatomy; immunofluorescence; calcium-binding proteins; parvalbumin

Introduction

Neuromodulation of neocortical circuits by acetylcholine (ACh) is a candidate mechanism for aspects of arousal and attention in mammals (Muir et al., 1994; Sarter et al., 2005). In the neocortex, ACh is usually released from varicosities that are not apposed to a synaptic specialization (Aoki and Kabak, 1992; Beaulieu and Somogyi, 1991; Umbriaco et al., 1994), a mode of release known as volume transmission (but see Turrini et al., 2001). Volume transmission implies that any specificity in ACh effects upon cortical circuits is likely to be conferred by selective expression of ACh receptors (AChRs). Data from both anatomical (Disney and Aoki, 2008; Disney et al., 2007; Disney et al., 2006) and physiological (Disney et al., 2007; 2012) studies show that, in the primary visual cortex (area V1) of the macaque monkey, cholinergic modulation is strongly targeted towards cortical inhibition. In particular, the vast majority of parvalbumin-immunoreactive (PV-ir) neurons in macaque V1 express the m1-type (pirenzepine-sensitive, Gq-coupled) muscarinic AChR (Disney and Aoki, 2008). In contrast, previous physiological data suggest that PV-ir neurons in the neocortex of rats rarely express pirenzepine-sensitive muscarinic AChRs (Gulledge et al., 2007; Kawaguchi, 1997; Kruglikov and Rudy, 2008).

These data raise the possibility of species differences in the targets for cholinergic neuromodulation in the neocortex. Interestingly, the PV-ir population itself is known to differ both between species and between cortical areas within species. In area V1 of the macaque monkey, 74% of GABAergic interneurons express PV (Van Brederode et al., 1990). This contrasts with PV expression in macaque prefrontal cortex and in the rodent neocortex, where only 50% of GABAergic neurons express PV (Conde et al., 1994; Gonchar and Burkhalter, 1997). Area V1 in macaques is also anatomically unique in other ways, including in its inhibitory neuronal population's composition, density and distribution.

Corresponding author: Anita Disney, Systems Neurobiology Laboratories, The Salk Institute for Biological Studies, 10010 North Torrey Pines Rd, La Jolla, California, 92037. Ph: (858) 453-4100. anita@salk.edu.

Conflict of Interests: None declared.

Role of Authors: All authors had full access to all the data in the study and take responsibility for the integrity of the data and the accuracy of the data analysis. Study concept and design: AD. Acquisition of data: AD. Analysis and interpretation of data: AD. Drafting of the manuscript: AD. Statistical analysis: AD. Obtained funding: AD & JHR. Study supervision: AD.

For example throughout the rest of the macaque neocortex, GABAergic interneurons comprise approximately 25% of the neuronal population, compared to only 20% in V1 (Beaulieu et al., 1992) and the composition of that population also differs from nearby visual areas (DeFelipe et al., 1999). V1 also has a higher density of cell bodies in all primates than do other cortical areas (Collins et al., 2010) as well as smaller dendritic fields and a lower density of spines (Elston and Rosa, 1997). It is thus not clear, when a difference is observed between macaque V1 and another cortical model system, whether that difference should be viewed as a feature of the species or of the cortical area.

Current models of visual processing are relatively well-developed (compared with other sensory modalities) and visual tasks are often used in experiments designed to examine higher cognitive functions such as those subserving reward and motivation, attention and memory. Existing visual cortical models have been developed based primarily on experiments conducted in carnivores (cats and ferrets) and primates (largely humans, macaques and marmosets) and have strongly emphasized the primary cortex of these species. However, the power of genetic techniques has led to an increase in the use of rodent models for studying the neocortex. Species differences in visual cortical anatomy and function need to be understood in this context in order to make the most appropriate use of the data arising from the various model systems currently in use.

To examine further the possibility of species differences in the cholinergic effectors for the primary visual cortex, the expression of m1 muscarinic AChRs by PV-ir neurons in area V1 was compared between rats, guinea pigs, ferrets, macaques and humans. Originally it was planned to examine V1 from mice as well, however the antibody controls failed in this species. The vast majority (74–85%) of PV-ir neurons in macaques, humans and guinea pigs express m1 AChRs. In contrast, in rats only 27% - and in ferrets 41% - of the PV-ir population are immunoreactive for m1 AChRs. These data largely agree with the results of physiological studies which have reported profound effects of cholinergic modulation on PV neurons in guinea pigs (McCormick and Prince, 1986) but not in rats (Gulledge et al., 2007; Kawaguchi, 1997). However, the data also reveal that while they do so much less frequently than in primates, PV-ir neurons in rats do express Gq-coupled muscarinic AChRs, which appear to have gone undetected in the previous *in vitro* studies (cited above, and others) of intrinsic membrane properties and synaptic transmission.

Materials and Methods

Histological preparation

The tissue used in this study came from a number of sources, a summary of tissue sources and fixation conditions is given in Table 1. Two (of three) rats, nine knockout mice (those generously provided by J. Wess), and all of the guinea pigs, ferrets and macaques were perfused by the one of the authors (AD) - details of these procedures are given below. The remaining four mice (two knockout and two wild type, generously provided by N. Nathanson), and one rat were perfused by the donor laboratories. All procedures and perfusions, by authors and donors, were performed in accordance with Institutional Guidelines for the Care and Use of Animals.

Rats—Three adult male Long Evans rats (*Rattus norvegicus*) were used in this study, two of which were perfused by the following method. Anesthesia was induced with 4% isoflurane and then rats were euthanized by i.p. injection of Euthasol (2cc). Once respiration had ceased, animals were transcardially perfused with 300mL of chilled, heparinized .01M phosphate-buffered saline (PBS; pH 7.4), followed by 400mL freshly prepared, chilled 4% paraformaldehyde (PFA) in 0.1M phosphate buffer (PB: pH 7.4). The brains were then removed and post-fixed in 4% PFA at 4°C overnight before being transferred to 30%

sucrose in PBS as a cryoprotectant. Once the brains had sunk, they were sectioned in the sagittal plane at 50μm on a freezing microtome. The third rat was exsanguinated with saline, perfused with 4% PFA, and sectioned by the donor laboratory (Chichilnisky laboratory, Salk Institute). A one-in-six series of sections for each animal was set aside for a Nissl reference set and the remaining tissue transferred to PBS with .05% sodium azide added for storage at 4°C.

Guinea pigs—Four adult male pigmented guinea pigs (*Cavia porcellus*) were used in this study. Anesthesia was induced with 4% isoflurane and maintained by a single i.p. dose of ketamine (75mg/kg) and xylazine (5mg/kg). Once corneal and pedal reflexes were abolished, animals were transcardially perfused with 500mL of chilled, heparinized PBS, followed by 300mL freshly prepared, chilled 4% PFA in PB. The brains were then removed and post-fixed in 4% PFA at 4°C overnight before being transferred to 30% sucrose in PBS as a cryoprotectant. Once the brains had sunk, they were sectioned in the coronal plane at 50μm on a freezing microtome. A one-in-six series of sections was set aside for a Nissl reference set and the remaining tissue transferred to PBS with .05% sodium azide added for storage at 4°C.

Ferrets—Three adult male ferrets (*Mustela putorius*) were used in this study. Anesthesia was induced with 4% isoflurane and then animals were euthanized by i.p. injection of Euthasol (3cc). Once respiration had ceased, animals were transcardially perfused with 5–600mL of chilled, heparinized PBS, followed by 700mL freshly prepared, chilled 4% PFA in PB. The brains were then removed and postfixed in 4% PFA at 4°C overnight before being transferred to 30% sucrose in PBS as a cryoprotectant. Once the brains had sunk, they were sectioned in the coronal plane at 50μm on a freezing microtome. A one-in-six series of sections was set aside for a Nissl reference set and the remaining tissue transferred to PBS with .05% sodium azide added for storage at 4°C.

Macaques—Four adult male rhesus macaque (*Macaca mulatta*), one adult male cynomologous monkey (*Macaca fascicularis*) and one adult male pig-tailed macaque (*Macaca nemestrina*) were used in this study. Animals were euthanized by i.v. injection of sodium pentobarbital (65 mg/kg). Following complete abolition of corneal and pedal reflexes (*mulatta*), or EEG determined brain death (*fascicularis*, *nemestrina*) animals were transcardially perfused with ~1000mL of chilled, heparinized PBS followed by freshly prepared, chilled 4% PFA in PB. The fixative was run for 30–40 minutes. The brains were then removed and blocked with a sagittal cut along the longitudinal fissure and a coronal cut at the anterior tip of the intraparietal sulcus. These blocks were post-fixed in 4% PFA at 4°C overnight before being transferred to 30% sucrose in PBS as a cryoprotectant. Once the tissue had sunk, the region from the anterior intraparietal sulcus to occipital pole were sectioned in the coronal plane at 50μm on a freezing microtome. Three, one-in-six series of sections were set aside; one for a Nissl reference set, another for a Gallyas reference set (Gallyas, 1970), and the third for a cytochrome oxidase reference set (Wong-Riley et al., 1998). The remaining tissue was transferred to PBS with .05% sodium azide added for storage at 4°C.

Human tissue—Five samples of human brain tissue were provided from the collection of control tissue (i.e. no pre- or post-mortem evidence of neurological disorder or dementia) by the Northwestern Alzheimer's Disease Center (NADC). Demographics, including postmortem interval (PMI), are presented in Table 2. Brains were removed at the NADC and each hemisphere cut into 2–4cm blocks. These blocks were fixed in 4% PFA at 4°C for 30 hours and then taken through a sucrose gradient to 40% sucrose with 0.02% sodium azide added. Blocks containing the cuneus gyrus, approximately 4–5cm from the occipital pole

were shipped in a small volume of PBS with 40% sucrose and .02% sodium azide added. Upon arrival, we sectioned the blocks at 50μm on a freezing microtome. Two one-in-six series of sections was set aside for Nissl and cytochrome oxidase reference sets and the remaining tissue transferred to PBS with .05% sodium azide added for storage at 4°C.

m1/3/5 knockout mice – Wess lab—Nine male C57BL/6 mice (three of each genotype: m1−/−, m3−/− and m5 −/−) were generously donated by J. Wess (NIH). These animals were euthanized by CO_2 inhalation. Once respiration had ceased, animals were transcardially perfused with 50mL of chilled, heparinized PBS, followed by 50mL freshly prepared, chilled 4% PFA in PB. The brains were then removed and post-fixed in 4% PFA at 4°C overnight before being transferred to 30% sucrose in PBS as a cryoprotectant. Once the brains had sunk, they were sectioned in the sagittal plane at 50μm on a freezing microtome. A one-in-six series of sections was set aside for a Nissl reference set and the remaining tissue transferred to PBS with .05% sodium azide added for storage at 4°C.

m1 knockout and wild type mice – Brains of two wild type and two m1AChR−/− null mice were generously donated by N. Nathanson (University of Washington). At the donor lab, the animals were exsanguinated with saline, perfused with 4% PFA and after post-fixation, whole brains were shipped in PBS with .05% sodium azide added. Upon arrival, we transferred blocks to 30% sucrose in PBS as a cryoprotectant. Once the brains had sunk, they were sectioned in the sagittal plane at 50μm on a freezing microtome. A one-in-six series of sections was set aside for a Nissl reference set and the remaining tissue transferred to PBS with .05% sodium azide added for storage at 4°C.

Source and Characteristics of Primary Antibodies

Please see Table 3 for a summary of the antibodies used in this study.

The monoclonal anti-parvalbumin used in this study is a mouse IgG1 produced by hybridization of mouse myeloma cells with spleen cells from mice immunized with purified parvalbumin from carp muscle (ms anti-PV: Cat # 235, lot 10–11(F); Swant Bellinzona, Switzerland). A number of polyclonal antibodies directed against the m1 acetylcholine receptor were screened for use in this study. Only one passed control in the key species of interest (rats and macaques). This antibody also passed controls for use in guinea pigs, ferrets and humans Data collection proceeded with an antibody raised in rabbit and directed against amino acids 227–353 of the human m1 muscarinic acetylcholine receptor (rb anti-m1: Cat#AMR-001, lot AN-05; Alomone labs, Jerusalem, Israel). Some of the other antibodies we tested (provided by different manufacturers) were directed against this same epitope, but failed controls. See *Antibody Controls*, below for details of control experiments.

A companion study to investigate Gq-coupled receptor sub-type substitution was planned to accompany the reported data. Antibodies directed against various epitopes on the m3 and m5 muscarinic ACh receptors were screened using knockout mice and preadsorption controls. None of the antibodies passed controls.

Antigen retrieval

Antigen retrieval was used to increase the yield (immunoreactive cell bodies per unit area) and to make identification of immunoreactive neurons easier in the human tissue. Sections were incubated in 1mM EDTA for 30 minutes at room temperature on a shaker. The vials of tissue were then placed in a water bath set at 80–95°C for 30 minutes. After removal from the water bath and 10 minutes of cooling, sections were transferred to room temperature 1mM EDTA for a 10-minute incubation on a shaker. These steps were followed by three 5-minute rinses in PBS, at which point the tissue was ready for antibody processing. This

procedure increased the number of visible immunoreactive neurons per tissue section and made staining easier to distinguish from background (Fig. 1) but did not alter the data on the proportion of dually labeled neurons. 243 parvalbumin-immunoreactive (PV-ir) neurons were counted in human tissue sections (from all five subjects) that did not undergo antigen retrieval. On average, 81.4% of these PV-ir neurons were dually labeled for the m1 muscarinic ACh receptor (m1-ir, N=5 human subjects, sd 8.5%). This did not differ significantly from the result for the 602 PV-ir neurons encountered in the tissue that did undergo antigen retrieval, of which 88.6% (sd 4.7%) were m1-ir. Thus the data were combined to give 845 PV-ir neurons in total. Antigen retrieval was only performed when immunoreactivity was to be visualized by immunofluorescence (and not when visualized by ABC-DAB) and was done in order to make the best use of the small number of human tissue sections available. The exception to this was in conducting preadsorption controls in which ABC-VIP visualization was used. Antigen retrieval did not noticeably increase neuropil immunoreactivity and was not done for any other species. The mouse anti-PV and rabbit anti-m1 antibodies passed preadsorption controls (see *Antibody Controls*, below) on human tissue both with and without water bath heat treatment antigen retrieval. The anti-m1 antibody did not pass pre-adsorption control following microwave irradiation.

Immunoperoxidase labeling

Tissue sections were processed to detect immunoreactivity for PV and for m1 muscarinic ACh receptors (mAChRs) using the ABC method. Sections for each species were always co-processed with tissue from at least one other species (usually three or four species per processing "batch" – a batch being the sections in a single well). The species that were processed together varied from batch to batch. Two or three sections per individual were chosen pseudorandomly from the tissue remaining after removal of sections for reference sets. First, the tissue was incubated in 0.3% hydrogen peroxide in 75% methanol for 20 minutes. Then, after three 5-minute rinses in PBS, the tissue was incubated for 1–2 hours in a blocking solution that comprised 1% IgG-free bovine serum albumin (BSA; Jackson ImmunoResearch), 5% normal goat serum (NGS; Jackson ImmunoResearch), 0.5% Triton X-100 (Triton) and 0.05% sodium azide, diluted in PBS. Primary antibodies were all diluted in blocking solution. The mouse anti-PV was diluted at 1:5000, the rabbit anti-m1 at 1:1500. After blocking, the tissue sections were transferred into the diluted primary antibody and incubated overnight at room temperature on a shaker.

The following day, after three 20-minute rinses in PBS, the sections were incubated for 1–2 hours in a biotinylated F'ab fragment secondary antibody. Secondary antibodies were diluted in PBS containing 1% BSA. The mouse anti-PV was detected using a goat anti-mouse IgG at 1:1000 (Jackson ImmunoResearch; Cat# 115-066-003, lot 76905); the rabbit anti-m1 using a goat anti-rabbit IgG at 1:2000 (Jackson ImmunoResearch; Cat# 111-066-003, lot 70900). Following this incubation and after three 5-minute rinses in PBS, the sections were incubated in an avidin-horseradish peroxidase complex (Vectastain Elite ABC kit, Vector Laboratories) at room temperature on a shaker for 30–60 minutes. Another three 5-minute rinses followed, before the tissue was transferred into VIP staining solution (Vector Labs). Staining proceeded for variable time periods (usually 2–8 minutes) and was terminated by PBS rinsing when visual inspection under a microscope indicated good visibility of the immunoreactivity had been achieved on a low background. Sections were then mounted and dried overnight before dehydration and coverslipping (Permout, Fisher).

Immunofluorescence, Dual-labeling

Dual immunofluorescence labeling was used to visualize both m1 AChRs and PV. As with the single labeling described above, sections from one species were co-processed (i.e. in the same well) with tissue sections from at least one other species and the specific combinations

of species varied from batch to batch. This method of controlling for processing differences was not used for two of the six macaque monkeys. The data from macaque tissue co-processed with other species did not differ from that for macaque tissue processed alone, and both replicate our previously reported result (Disney and Aoki, 2008). Thus data from macaque tissue processed alone and macaque tissue processed with other species have been combined. On the day of staining, two sections from each individual were selected pseudorandomly and incubated in blocking solution for 1–2 hours. For immunofluorescence staining, the mouse anti-PV was used at 1:1000 and the rabbit anti-m1 at 1:800 in blocking solution. Sections were co-incubated for 24–72 hours, at room temperature on a shaker, in both antibodies concurrently. After thorough rinsing, sections were transferred into secondary antibodies (again, co-incubated in a single processing step). Secondary antibodies were diluted in PBS with 1% BSA added. The mouse anti-PV was detected using a Dylight 488 conjugated donkey anti-mouse IgG (Jackson ImmunoResearch; Cat# 715-486-150, lots 93947 & 95844), the rabbit anti-m1 with a Dylight 594 conjugated donkey anti-rabbit IgG (Jackson ImmunoResearch; Cat# 711-516-152, lots 97356 & 92916). The tissue was incubated at room temperature on a shaker, protected from light, for 6–24 hours. Following thorough rinses, the sections were mounted, dried overnight in the dark and then dehydrated and coverslipped (DPX, Electron Microscopy Services).

Antibody controls, primary antibodies

The antibody directed against PV has been shown previously to be specific by immunoblot of mouse brain and muscle extract (Celio et al., 1988) and does not label tissue from PV knockout mice (Schwaller et al., 1999).

The antibody directed against the m1 AChR labels a single 78 kD band on western blots of rat brain (manufacturer product insert) and macaque brain (Disney et al., 2006).

We performed preadsorption controls on all antibodies, in all species. For the human tissue this control was undertaken for sections that had undergone antigen retrieval as well as sections that had no such pre-treatment. The peptide for the m1 preadsorption control was provided by the manufacturer (Alomone Labs). The protein for the parvalbumin preadsorption was a purified rat recombinant parvalbumin produced in *E. coli* (Swant, lot 5.’93).

When diluting the control antigens, a 40-fold molar excess (relative to IgG concentration of the antibody) was used for the rabbit anti-m1 antibody preadsorption, and a 25-fold molar excess for the mouse anti-PV. The primary antibodies were used as described in the section on immunoperoxidase labeling and effectiveness of preadsorption was assessed by the ABC-VIP method, as described above. Antibodies were pre-incubated with their respective antigens for 2–3 hours at room temperature on a shaker. The preadsorbed antibodies were then used as-is (i.e. without centrifugation or filtration). Preadsorption eliminated staining by both antibodies in all species tested **except mice.** In the other species we observed normal patterns of immunoreactivity in sections processed simultaneously according to the normal protocol, but little to no staining in sections that were simultaneously processed using a preadsorbed antibody.

The rabbit anti-m1 used in this study did label homozygous null m1 “knockout” mice (from both the Wess and Nathanson labs). However, this antibody also failed the preadsorption control in mice, both wild type and m1 −/−. These data indicate that this lot (AN-05) of the Alomone rabbit anti-m1 antibody (which is directed against an epitope from the human m1 AChR) interacts non-specifically with unidentified protein targets in mice but not in the other species used in this study. It is thus unsurprising that the antibody also labels tissue from knockout mice: the antibody’s failure in the knockout control is explicable in the

context of the preadsorption control. The fact that this antibody passes preadsorption controls in the other species tested and fails the same control in mouse, argues for its specificity in the species here tested (rat, guinea pig, ferret, macaque, human) and against the use of the knockout mouse control to evaluate this antibody in species other than mouse. Interestingly, while staining was completely abolished by preadsorption in guinea pigs, ferrets, macaques and humans, a weak residual immunoreactivity was present in the rat, indicating that some level of non-specific interaction may occur in this rodent species as well. When the preadsorption control was conducted using immunofluorescence (IF) detection, the residual staining in rat was undetectable and thus will not have interfered with the quantification presented in this study. Switching to IF detection did not reduce the visible immunoreactivity in the mouse tissue.

It should be noted that a different lot of antibody from Alomone labs passed and failed controls in a different pattern across species. A polyclonal anti-m1 antibody from Millipore also passed in a lot-specific fashion in some species (no lot from Millipore ever passed controls for use in rat, leading to its exclusion from this study), indicating variability in performance of these antibodies and highlighting the need for controls on every new lot of antibody.

Antibody controls, secondary antibodies

For each batch of processing, a control condition was included to confirm the specificity of the secondary antibodies. This involved incubating tissue sections in solutions without primary antibodies (no primary control). In these controls, sections were incubated in blocking solution for the same duration as the companion (fully processed) sections were exposed to the primary antibody. All sections were subsequently processed identically, according to the regular protocols. In the one case where this incubation produced a fluorescent signal, all of the tissue processed in that batch was discarded.

Control experiments were also conducted in which tissue sections that had been incubated with a primary antibody were subsequently processed in a solution containing a secondary antibody. The secondary antibody targeted a different species than the host animal in which the primary antibody was raised (mismatched secondary control). In other words, the secondary antibody had no target epitope in the tissue. This procedure produced no fluorescent signal.

Confocal microscopy

Data was collected from the primary visual cortex (V1), Brodmann area 17 (Brodmann, 1909). V1 was identified in all species using Nissl-stained reference sections, aided by brain atlases and published data (Choudhury, 1978; McConnell and LeVay, 1986; Paxinos and Franklin, 2003; Paxinos et al., 2000; Paxinos and Watson, 2007; White et al., 1999). The proportion of PV neurons that were immunoreactive for m1 AChRs did not differ by layer in any species in this study (see Results) as in our previous study (Disney and Aoki, 2008). Counts are therefore reported for layers 2 & 3 (combined), layer 4 (4c in humans and macaques), layer 5 and layer 6. Layers 4a and 4b were counted in macaques and humans but did not differ from each other or from layer 4c (within species) these data are omitted from the graphs in Figure 2 but are included in Table 5.

Using a Zeiss LSM 710 laser scanning confocal microscope, image montages were collected using the ‘Tile Scan’ function. For each new tissue section, laser power was chosen independently for each laser line such that with a given the laser line turned off no image was captured in the corresponding data channel. Laser power was independently determined for each tissue section. Between two and five V1 regions were imaged per tissue section. For

each imaged region, two z-axis "stacks" were first collected using a 40x water immersion objective. The first was taken just below the layer 1/2 border (i.e. in layer 2) and the other just above the layer 6/white matter border (i.e. in layer 6). Using these stacks, an imaging plane was selected such that all cortical layers would be present in a single z-axis imaging plane. These stacks were also used to determine the average tissue thickness measure used in the Abercrombie correction for non-stereological quantification (see below) and to confirm antibody penetration throughout the thickness of the tissue. Once an imaging depth was selected, a 210–215 μm-wide scan was taken that captured the entire thickness of cortex from pia to white matter. Images were captured to two data channels concurrently, using the same 40x water immersion objective, with a pinhole size of 35.8 (~1 AU). Overview scans centered on the same region with a width of 630–640 μm, aided with registration of the confocal scans with adjacent Nissl reference sections.

Determining layer boundaries

For each immunolabeled section, an adjacent Nissl reference section was used to determine layer boundaries. Digital images of the reference sections were taken with a Zeiss Axio Observer VivaTome microscope, using a 25x objective and focusing on the region adjacent (in the 'z axis') to each data scan. Co-registration of the fluorescence and light microscopic images was achieved using gross morphology, pial surface shape, cutting and other artefacts, and blood vessels, as fiduciary marks. The depths - in microns from the pial surface - of layers 4 (4a, b, and c in human and macaque), 5, and 6 were recorded on the reference images. These measurements were then converted to the magnification of the data images and the layer boundaries drawn with a +/− 10 μm confidence boundary. The depth of the boundary between layers 1 and 2 was determined by eye based on the sharp increase in the density of somata at the layer transition. Layer borders were confirmed by comparison with the staining profile for PV in which an intense band of immunoreactivity can be seen corresponding to layers 4 and 6 (4c and 6 in humans and macaques).

Counting cells

Layer boundaries were drawn onto TIFF image files of the stitched together to form Tile Scans using Photoshop (Adobe). Counting was done using custom software written in Matlab (Mathworks). Data channels (red or green) were isolated and identified somata counted separately from gray-scale images. Only wholly visible, in focus somata were counted. Somata that crossed the image boundary or the 20 μm confidence boundary around layer borders were excluded, as were objects smaller than 5 μm along their long axis. The x and y coordinates of the center of the cell body were recorded. Quantifications were made from small shapes (equivalent to a 5 micron object) centered at these x/y co-ordinates in a new image frame, i.e. in the same frame size but with the data channels turned off. The counting objects had to overlap to be counted as dually labeled. In cases where the markings touched but did not overlap, the data channels were inspected and a qualitative determination was made. Less than 0.2% of the sample required this additional step.

It is important to note that this study was not designed to be fully stereological in nature. In particular, tissue sections selected for processing were chosen pseudo-randomly from the set of V1 sections available for a given animal rather by systematic-random methods. Additionally, we did not have access to the whole of V1 for any human subject. Our counts are therefore not exhaustive; they reflect the local densities in the counted regions and should not be taken as an unbiased representation of cell densities across the entire visual field representation in any species.

Qualitative data collection

Qualitative observations were made from both the immunoperoxidase stained tissue and from the photomicrographs used to collect quantitative data. For non-somatic staining the term 'neuropil staining' will be used. Neuropil staining includes axonal, dendritic, and punctate labeling. Axons were identified according to the presence of clearly distinguishable varicosities resembling 'beads on a string' (See Figures 4, 6 and 7 for clear examples of axonal labeling). Dendrites were identified as processes of a slightly varicose or non-varicose nature. Additionally, we identified puncta as small spots, ~1μm or less, that were not clearly attached to a neuronal process. These puncta could represent spines, axon terminals or 'islands' of immunoreactivity along larger processes such as dendrites or axons.

Photomicrograph Production

Light micrographs were captured using a Zeiss CCD camera and AxioVision software. Brightness and contrast settings were chosen using a live color image. The brightness and contrast were deemed optimal when the lumen of any visible vasculature appeared white, the reaction product appeared to be the same intensity as was observable under the compound microscope and when histograms of the color intensities were well-matched across channels. Gamma correction was not used. Images were viewed offline using Photoshop (Adobe) software. Unless noted in the figure legend, no alterations were made prior to publication

Confocal images were captured using the Zeiss Zen 2010 software package. Brightness and contrast settings were chosen using a live (false color) image and were set such that the lumen of any visible vasculature appeared black and to minimize saturation. Gamma correction was not used. Unless noted in the figure legend, the only alterations made for publication were to convert the red/green data images to magenta/green.

Analysis

This study was not stereological by design, so the Abercrombie correction (T/T+h: see (Guillery, 2002) was applied to reduce the counting bias associated with soma size. Object height (h) was measured as the average diameter along the long axis of the cell soma for a random sample of ten neurons across all layers from at least two tissue sections per species. The mean values for h are listed for each cell type and species in Table 4.

To determine a value for T, the mean dehydrated thickness of the tissue was measured as the distance between the upper- and lower-most in-focus planes in one of the z-stacks taken at the beginning of each scan (see Confocal microscopy, above). The obtained values for T (measured across 6–10 sections per species) were: rat 36.6μm (sd 2.9), guinea pig 34.1μm (sd 4.1), ferret 32.6μm (sd 2.2), macaque 34.7μm (sd 3.46), and human 31.9μm (sd 2.7).

The resulting Abercrombie correction factors for PV neurons were: rat V1 0.70, rat S1 0.68, guinea pig 0.67, ferret 0.66, macaque 0.73, and human 0.67. For m1 the correction factors were rat V1 0.69, rat S1 0.69, guinea pig 0.66, ferret 0.64, macaque 0.72, and human 0.66. Both raw and corrected counts are reported in the text, all percentages are calculated based on the corrected numbers.

Results

The main purpose of this study is to determine the extent to which species differences exist in the proportion of PV-ir neurons in area V1 that area also immunoreactive for the m1-type muscarinic acetylcholine receptor. The differences are in fact striking and exist even when

tissue sections from all species are co-processed in a single well (i.e. processing conditions are as identical as possible for such a study).

2326PV-ir neurons were counted across V1 of five species: rat, guinea pig, ferret, macaque and human. The raw and Abercrombie-corrected counts and resulting percentages collapsed across all cortical layers are presented in Table 4. It can be seen that while guinea pigs, macaques and humans all show high levels of m1 AChR expression across the PV-ir population (76–85% of PV-ir neurons dual labeled), in ferret V1 far fewer PV-ir neurons are m1AChR-ir (41%) and this percentage is lower still for rat V1 (27%). A comparison with the primary somatosensory cortex in the rat indicates that this low level is not specific to V1, in area S1 of the rat only 21% (sd 12.5) of PV-ir neurons are also immunoreactive for m1AChRs (57 of 233, 39.04 of 158.44 corrected).

While brain death and exposure of the tissue to fixative occurred within a short period of time for non-human species, post-mortem interval (PMI) was much higher for the human subjects, ranging from four to twelve hours across individuals. Table 2 shows the total number of PV neurons counted and the proportion of those neurons that were immunoreactive for m1 AChRs for each individual. While the individual with the shortest PMI (4 hours) did show the highest degree of dual labeling (89%) overall there is no correlation between percent dual labeling and PMI ($r=-0.747$, $p=.07$) or age ($r=0$) across the human subjects.

A laminar profile for the dual labeling in each species is presented in Figure 2. In all species the proportion of PV-ir neurons that are also immunoreactive for m1AChRs is roughly constant across layers, with perhaps slightly lower dual labeling for PV-ir neurons in the layer 6 of the guinea pig.

Single label immunoreactivity profiles

Immunoreactivity for parvalbumin fills much of the cell (soma, dendrites and axon) in many, if not all, individual immunopositive cells and has a laminar profile in the neocortex (Figure 3). There is a higher apparent density of neurons and often a darker staining of the neuropil in layer 4 (4a and 4c in macaques and humans) and usually in layer 6 also. This neuropil immunoreactivity, particularly apparent in human layer 4c (Fig. 3E), was not noticeably increased by antigen retrieval (compare panels B and D of Fig. 1). A similar broad laminar pattern is evident in all of the species studied here, but there were some variations across species and subtle differences across individuals. The general laminar pattern appeared stronger in macaques and humans and was weakest in ferrets. PV-ir neurons were almost never seen in layer 1, though Figure 4 shows a large PV-ir neuron encountered in layer 1 of the peripheral visual field representation (>10 degrees eccentricity) of macaque V1.

Somatic staining for parvalbumin was consistently fainter and neuropil staining more diffuse in guinea pigs than in the other species studied here (Figure 3). This was true even in test experiments in which a higher concentration of antibody was used in the primary incubation (up to 1:250 for immunofluorescence and 1:400 for immunoperoxidase).

The qualitative detail of m1 immunoreactivity also differs between species. In both rats and ferrets, in which the proportion of dually labeled PV-ir neurons is lowest, there is stronger neuropil immunoreactivity than in the guinea pigs, macaques or humans (Figure 5). The lower contrast difference between the somata and the neuropil evident in the panels for the rat and the ferret in Figure 5 is not a reproduction error, nor evidence for needed image correction; this is how the tissue appears when viewed under the microscope.

The somatic m1 immunoreactivity, on the other hand, is similar across species - a stained cytoplasmic ring around an immunonegative nuclear region with some labeling of the proximal dendrites (Figures 5, and 6). In ferrets and rats, this somatic staining was less intense than in guinea pigs, macaques or humans. In layer 4b of macaques and humans, there are large, intensely m1-immunopositive somata.

Dual label immunoreactivity profiles

The highly punctate nature of the non-somatic m1 immunoreactivity makes it difficult to determine whether the m1 receptors are localized to dendrites versus axons. At the resolution of these images even co-localization at the pixel level must be approached with caution as pre- versus post-synaptic localization cannot be determined with confidence. However, in the rare cases where there is a clearly m1-immunoreactive process (Figure 6), it is usually a dendrite. A quantification of these rare processes was not attempted but they seem more common in the ferret than in other species. There are certainly examples of processes that were dually labeled, and examples that are singly labeled (Figure 6) for m1 AChRs.

An example of clearly identifiable axonal segments in this tissue are the PV-ir baskets of axon terminals surrounding m1-ir and m1-negative somata. These are common in all species in which they could be evaluated (Figures 6A and 7) and appear to be immunonegative for m1 AChRs.

Neuropil PV antigenicity is not well-enough preserved by the immersion fixation protocol used in preparing the human samples to allow an assessment of m1 immunoreactivity in any PV-ir non-somatic compartments (Figure 7G–I). While there is punctate PV immunoreactivity, it is not associated with larger structures that would allow one to identify the puncta as being part of an axon or a dendrite. It is therefore possible that, while identifiable PV-ir axons in rats. ferrets, guinea pigs, and macaques were almost always clearly m1 ACh immunonegative, and m1 immunoreactivity was sparse on identifiable PV-ir dendrites, the same may not be true in V1 of humans.

Our previous study of m1 AChR expression by inhibitory and excitatory neurons in macaque V1 showed that fewer than 10% of excitatory neurons express the m1 receptor (Disney et al., 2006). This is clearly not the case for all species included in this study. Figure 8 shows dual labeling from layer 2 of three species; ferret (Fig. 8A,D), guinea pig (Fig. 8B,E), and human (Fig. 8C,F). While we did not attempt to quantify expression by excitatory neurons, the qualitative impression is that in both ferret and guinea pig V1, many neurons that are not immunoreactive for PV express m1 ACh receptors. These singly labeled m1 immunoreactive neurons from human V1 (Fig. 8F) appear sparser, of a smaller size, and seem to have a less distinctly “pyramidal” shape than do the singly labeled m1-immunoreactive neurons in ferret (Fig. 8D) or guinea pig (Fig. 8E). Interestingly, Figures 8B and E, combined with the graph showing a quantification of dual labeling for guinea pig (Fig. 2) suggest that guinea pigs may actually have uniquely high levels of m1 AChR expression overall; with most neurons expressing this receptor. This is unlike the ferret and the rat, in which expression by excitatory neurons appears high (Fig. 8A,B,D,E) but expression by parvalbumin-immunoreactive neurons is low (Fig. 2); and unlike humans and macaques in which expression by parvalbumin neurons is high (Fig. 2) but expression by excitatory neurons appears low (Fig 8C,F).

Discussion

This study shows that there are prominent species differences in the proportion of parvalbumin immunoreactive neurons in the primary visual cortex that express m1-type

muscarinic acetylcholine receptors. The species here studied can be clustered into two groups. In the case of the first group - comprising guinea pigs, macaques and humans – the vast majority (76% or more) of PV-ir neurons also express m1 ACh receptors. For the remaining two species, far fewer PV-ir neurons express these receptors, with 41% of PV-ir neurons in ferrets and only 27% in rats expressing m1 ACh receptors.

The possibility of membrane insertion in non-somatic compartments

The difference in neuropil immunoreactivity - in which the neuropil of rats and ferrets is more intensely immunoreactive than the neuropil of guinea pigs, macaques and humans - may indicate that there is a difference not only in the proportion of the PV-ir population that is m1-expressing, but also in the trafficking (or site of synthesis) of the receptors. The labeling intensity of immunoreactive somata is fainter in rats and ferrets, and the labeling intensity of the neuropil stronger, when compared with the other species. We observed clear cases of immunoreactivity in dendrites (Figure 6B, in ferret). This may indicate that the m1 AChRs being made by these cells are most likely to be membrane inserted in a non-somatic cellular compartment. Particularly if that were a dendritic compartment, this could explain why these receptors appear to have gone undetected in previous *in vitro* studies of cholinergic modulation of the intrinsic membrane properties of PV-ir neurons in rats (Gulledge et al., 2007; Kawaguchi, 1997; Kruglikov and Rudy, 2008). It should be noted here that muscarinic receptor-mediated polarization changes in PV-ir neurons were reported in one previous *in vitro* study of layer 5 neurons in rat V1 (Xiang et al., 1998), these conflicting studies are discussed further below.

It is possible that this evidence for membrane-insertion of m1 AChRs beyond the soma of PV neurons in rats and ferrets resulted in an underestimate of immunoreactive neurons in these species. This could occur if the receptors are rapidly trafficked out of the soma after synthesis, or if the receptors were in fact never in the soma, having been made in the dendrite. This can result in undetectable somatic immunoreactivity in a neuron that actually expresses a protein of interest (Burette et al., 2002). We have shown previously that, at least in macaques, counting somata does not underestimate the population of neurons immunoreactive for muscarinic receptors, even for receptor subtypes (such as the m2 receptor) that are rarely membrane inserted at the soma and are almost entirely trafficked out into the distal processes of the cell (Disney et al., 2006).

While apparent co-localization at the pixel level was evident in many images, particularly from ferret and rat V1, at the resolution of the images taken for this study such observations must be approached with caution as there is the real possibility that the close apposition of processes that occurs at a synapse can result in a false-positive dually labeled pixel. This can usually be ruled out in the case of immunoreactivity that traces out a section of a dendritic or axonal process (as is seen in Figures 6B&C), but this was usually not the case with the m1 immunoreactivity profile - which was typically highly punctate.

This question could be resolved by a future study of m1 receptor expression and localization at the electron-microscopic level. Even if such a study were to find that the majority of PV neurons in rat and/or ferret V1 expressed m1 AChRs, but did so in the dendrite or axon, the claim of a species difference would still stand. We have shown previously, by electron microscopy, that m1 ACh receptors are rarely expressed in distal processes (dendrites or axons) of *any* neurons in V1 of the macaque (Disney and Aoki, 2008; Disney et al., 2006).

A lack of dual immunoreactivity is a clearer result when, as is the case with parvalbumin, one of the labels essentially fills much of the cell. Thus the lack of dually immunolabeled varicosities in the PV-ir baskets can be taken as evidence that the release of GABA from these perisomatic structures is probably not modulated by ACh acting via m1 AChRs. It has

been shown previously that ACh, acting via m2 AChRs *does* modulate GABA release by PV cells (Kruglikov and Rudy, 2008).

Previous physiological findings

Our results fit well with a number of previous physiological findings. One of the earliest *in vitro* investigations of cholinergic modulation in the neocortex of mammals was a study of the cingulate cortex of guinea pigs (McCormick and Prince, 1986). In those experiments, it was shown that ACh depolarized fast-spiking neurons and caused those neurons to fire action potentials. The authors further showed that a late hyperpolarization seen in adjacent pyramidal neurons following ACh application could be blocked by the GABAa receptor antagonist bicuculline. The authors did not stain for parvalbumin in these fast-spiking neurons, but given their physiological properties it is likely that they were parvalbumin-immunoreactive neurons (Kawaguchi and Kubota, 1993). The authors did not determine which class of ACh receptors might underlie this effect; the present data suggest that somatic m1 receptors could well have played a role.

It has also been shown that when ACh has suppressive effects on spiking in macaque V1, these effects can also be blocked with a GABAa receptor antagonist (Disney et al., 2012). Given that 74% of GABAergic neurons in macaque V1 express parvalbumin (Van Brederode et al., 1990), and PV neurons frequently innervate the cell body of their target neurons (reviewed by (Markram et al., 2004) it is likely that the suppressive effects of ACh on visual responses observed *in vivo* were mediated largely by PV neurons, although other interneuron subtypes could be involved. PV neurons in macaque V1 express ACh receptors more strongly than do excitatory neurons or calbindin- or calretinin-immunoreactive inhibitory neurons, and PV neurons express m1 AChRs more strongly than m2 AChRs (Disney and Aoki, 2008; Disney et al., 2007). Disynaptic control of the level of inhibition - resulting from cholinergic activation of excitatory neurons that in turn drive inhibition – may add to direct effects on inhibitory neurons *in vivo*. However given that fewer than 10% of excitatory neurons in macaque V1 express muscarinic AChRs (Disney et al., 2006), this is unlikely to be a major contributing mechanism. Our finding that inhibition is a primary target for modulation of visual processing by ACh in macaques is also predicted by a recent model of cholinergic modulation in the context of a visual attention task (Deco and Thiele, 2011).

Thus in two of the three species that are here shown to have a large population of m1 ACh receptor-expressing PV neurons (macaques and guinea pigs), it has also been shown physiologically that ACh can induce GABA release and thereby induce suppressed firing of principal cells. Cholinergic modulation has not been studied in the ferret, but in rats it has been suggested by a number of *in vitro* studies that ACh does not depolarize PV neurons (which would be necessary for release of GABA as seen in guinea pigs and macaques). There has been some debate as to what ACh does do to PV neurons in rats *in vitro*. Two studies have shown no membrane polarization change (i.e. neither depolarization nor hyperpolarization) in PV neurons exposed to ACh (Gulledge et al., 2007; Kawaguchi, 1997). A third study reported that ACh could hyperpolarize PV neurons, and that it did so via muscarinic receptors. The muscarinic receptor subtype involved was not determined (Xiang et al., 1998). It has been shown that m2 muscarinic receptors are expressed by PV neurons in rat neocortex, and that they act in their well-described manner as presynaptic inhibitors of neurotransmitter release (Kruglikov and Rudy, 2008). If muscarinic receptors (m1 or m2 type) tend to be expressed in the axon or dendrites of PV neurons rather than at the soma - as is suggested by the weak somatic and strong neuropil staining we report – this could explain why their effects have generally been missed in studies of intrinsic membrane properties measured through *in vitro* whole cell patch recordings made at the soma.

Until recently there was no evidence that muscarinic receptors could act upon PV neurons in rodents in a manner similar to that which we have suggested above; i.e. that ACh depolarizes PV neurons as a result of m1 AChR activation and that this depolarization causes the release of GABA. We were unable to include mice in this study (due to problems of antibody specificity) but a recent paper shows that in the mouse visual cortex *in vivo* ACh released as a result of basal forebrain stimulation activates 25% of PV neurons, via muscarinic receptors, when the surrounding cortex is only weakly desynchronized (Alitto and Dan, 2012). This value of 25% corresponds impressively well with the 27% of PV neurons we report as expressing m1 AChRs in the rat visual cortex.

It is important to note here that while we have shown previously that only 10% of excitatory neurons in macaques express m1 AChRs (Disney et al., 2006), this is almost certainly not the case in all species. While we have not quantified m1 immunoreactivity by GABAergic and non-GABAergic neurons in V1 of any species other than the macaque (and these data are also not available in the literature to our knowledge), it is clear from an inspection of the figures presented here (particularly Figures 5–8) that excitatory neurons in other species frequently express these receptors. Thus it seems likely that a further species difference exists; namely the extent to which excitatory neurons express m1 AChRs. Quantitative anatomical confirmation of this would require a further study comparing dual labeling for m1 AChR with antibodies directed against either GABA (a study which would require different fixation conditions that were used in the present work) or against GAD 65/67 (which in our experience has a high detection failure) and a pan-neuronal marker such as an antibody directed against NeuN. Toccche suggestion is supported for the rat by an earlier report that between 25 and 95% (depending on cortical layer) of excitatory neurons respond to ACh (Gulledge et al., 2007). When expressed by excitatory neurons, m1 ACh receptors couple to the m-current (Brown and Adams, 1980), a potassium current that underlies spike frequency adaption. Activation of an m1 AChR with this coupling suppresses the m-current and thus increases spike rate. Thus whether net suppression or activation of cortex dominates following activation of m1 AChRs may well vary across species depending upon which classes of neurons express these receptors, and to what extent.

We have reported previously that 40% of calretinin-immunoreactive neurons and 60% of calbindin-immunoreactive neurons express the m1 ACh receptor (Disney and Aoki, 2008). Inhibitory neurons that are not immunoreactive for PV are often subdivided using different markers in rodents - such as the 5-HT3 serotonin receptor, somatostatin, cholecystokinin, and vasoactive intestinal peptide. While it is a matter of debate as to whether PV neurons in rat cortex respond to ACh (as discussed above), it has been shown that other interneuron types do depolarize in response to cholinergic agonists. Of particular note in this context is the observation that cholecystokinin-, and vasoactive intestinal peptide-immunoreactive neurons are depolarized by muscarine (Kawaguchi, 1997) and neurons such as bipolar and bitufted inhibitory neurons, which can express cholecystokinin or vasoactive intestinal peptide, can also often express calbindin or calretinin (reviewed by (Markram et al., 2004). Thus, it seems likely that these (and perhaps other) non PV-immunoreactive interneuron types in rodent cortex may often express m1 AChRs, as they do in the macaque.

Modulating cortical inhibition

How cholinergic modulation of inhibitory neurons, including PV-ir neurons might affect cortical function will depend upon the role one ascribes to cortical inhibition - a treatment of theories on the role of inhibition in cortex is beyond the scope of this discussion. It has been proposed by numerous investigators that cortical cholinergic modulation underlies attention (Arnold et al., 2002; Deco and Thiele, 2011; Hasselmo and McGaughy, 2004; Herrero et al., 2008; Himmelheber et al., 2000; McGaughy and Sarter, 1998; Sarter et al., 2005) and it has

also been argued that changes in GABAergic inhibition could account for response gain changes seen in V1 during attention tasks (Katzner et al., 2011). Despite the different anatomical circuits, ACh is suppressive in the rodent cortex (Gil et al., 1997; Hasselmo and Bower, 1992; Hsieh et al., 2000; Kimura, 2000) as it is in the macaque cortex (Disney et al., 2012) and ACh has been shown to boost thalamic gain in both species (Disney et al., 2007; Gil et al., 1997; Hasselmo and Bower, 1992; Hsieh et al., 2000; Kimura, 2000) and evidence for ACh's role in attention arises from studies of both species (Deco and Thiele, 2011; Herrero et al., 2008; Sarter et al., 2005). It is an intriguing possibility, warranting further investigation, that non-equivalent anatomical circuits may nonetheless be doing equivalent computations across species.

Acknowledgments

This work was supported by NIH grants K99 MH-93567 to AAD, R01 EY-021827 to JHR, NEI core grant for Vision research P30 EY19005 to the Salk Institute and by the Gatsby Charitable Foundation.

Human tissue used in this study was provided by the Northwestern ADC, P30 AG13854. We sincerely thank the donors of our non-human brain samples: J.A. Movshon, M. Hawken, J. Gottlieb, E. Callaway, E. Chichilnisky, J. Wess, and N. Nathanson. Thanks to H. Alasady and M. Yankowski for assisting in the preparation of the Nissl reference sets and to the staff at the Waitt Biophotonics imaging core at the Salk Institute for their invaluable technical support for the imaging.

References

Alitto HJ, Dan Y. Cell-type-specific modulation of neocortical activity by basal forebrain input. Frontiers in systems neuroscience. 2012; 6:79. [PubMed: 23316142]

Aoki C, Kabak S. Cholinergic terminals in the cat visual cortex: ultrastructural basis for interaction with glutamate-immunoreactive neurons and other cells. Visual neuroscience. 1992; 8(3):177–191. [PubMed: 1347700]

Arnold HM, Burk JA, Hodgson EM, Sarter M, Bruno JP. Differential cortical acetylcholine release in rats performing a sustained attention task versus behavioral control tasks that do not explicitly tax attention. Neuroscience. 2002; 114(2):451–460. [PubMed: 12204214]

Beaulieu C, Kisvarday Z, Somogyi P, Cynader M, Cowey A. Quantitative distribution of GABA-immunopositive and -immunonegative neurons and synapses in the monkey striate cortex (area 17). Cerebral cortex. 1992; 2(4):295–309. [PubMed: 1330121]

Beaulieu C, Somogyi P. Enrichment of cholinergic synaptic terminals on GABAergic neurons and coexistence of immunoreactive GABA and choline acetyltransferase in the same synaptic terminals in the striate cortex of the cat. J Comp Neurol. 1991; 304(4):666–680. [PubMed: 2013651]

Brodmann, K. Localisation in the cerebral cortex. Garey, LJ., translator. London: Smith-Gordon; 1909.

Brown DA, Adams PR. Muscarinic suppression of a novel voltage-sensitive K+ current in a vertebrate neurone. Nature. 1980; 283(5748):673–676. [PubMed: 6965523]

Burette A, Zabel U, Weinberg RJ, Schmidt HH, Valtschanoff JG. Synaptic localization of nitric oxide synthase and soluble guanylyl cyclase in the hippocampus. J Neurosci. 2002; 22(20):8961–8970. [PubMed: 12388603]

Celio MR, Baier W, Scharer L, de Viragh PA, Gerday C. Monoclonal antibodies directed against the calcium binding protein parvalbumin. Cell Calcium. 1988; 9(2):81–86. [PubMed: 3383226]

Choudhury BP. Retinotopic organization of the guinea pig's visual cortex. Brain Res. 1978; 144(1): 19–29. [PubMed: 638761]

Collins CE, Airey DC, Young NA, Leitch DB, Kaas JH. Neuron densities vary across and within cortical areas in primates. Proceedings of the National Academy of Sciences of the United States of America. 2010; 107(36):15927–15932. [PubMed: 20798050]

Conde F, Lund JS, Jacobowitz DM, Baimbridge KG, Lewis DA. Local circuit neurons immunoreactive for calretinin, calbindin D-28k or parvalbumin in monkey prefrontal cortex: distribution and morphology. J Comp Neurol. 1994; 341(1):95–116. [PubMed: 8006226]

Deco G, Thiele A. Cholinergic control of cortical network interactions enables feedback-mediated attentional modulation. The European journal of neuroscience. 2011; 34(1):146–157. [PubMed: 21692884]

DeFelipe J, Gonzalez-Albo MC, Del Rio MR, Elston GN. Distribution and patterns of connectivity of interneurons containing calbindin, calretinin, and parvalbumin in visual areas of the occipital and temporal lobes of the macaque monkey. J Comp Neurol. 1999; 412(3):515–526. [PubMed: 10441237]

Disney AA, Aoki C. Muscarinic acetylcholine receptors in macaque V1 are most frequently expressed by parvalbumin-immunoreactive neurons. J Comp Neurol. 2008; 507(5):1748–1762. [PubMed: 18265004]

Disney AA, Aoki C, Hawken MJ. Gain modulation by nicotine in macaque v1. Neuron. 2007; 56(4): 701–713. [PubMed: 18031686]

Disney AA, Aoki C, Hawken MJ. Cholinergic suppression of visual responses in primate V1 is mediated by GABAergic inhibition. J Neurophysiol. 2012

Disney AA, Domakonda K, Aoki C. Differential expression of muscarinic acetylcholine receptors across excitatory and inhibitory cells in visual cortical areas V1 and V2 of the macaque monkey. Journal of Comparative Neurology. 2006; 499(1):49–63. [PubMed: 16958109]

Elston GN, Rosa MG. The occipitoparietal pathway of the macaque monkey: comparison of pyramidal cell morphology in layer III of functionally related cortical visual areas. Cerebral cortex. 1997; 7(5):432–452. [PubMed: 9261573]

Gallyas F. Silver staining of micro- and oligodendroglia by means of physical development. Acta neuropathologica. 1970; 16(1):35–38. [PubMed: 4195517]

Gil Z, Connors BW, Amitai Y. Differential regulation of neocortical synapses by neuromodulators and activity. Neuron. 1997; 19(3):679–686. [PubMed: 9331357]

Gonchar Y, Burkhalter A. Three distinct families of GABAergic neurons in rat visual cortex. Cerebral cortex. 1997; 7(4):347–358. [PubMed: 9177765]

Guillery RW. On counting and counting errors. J Comp Neurol. 2002; 447(1):1–7. [PubMed: 11967890]

Gulledge AT, Park SB, Kawaguchi Y, Stuart GJ. Heterogeneity of phasic cholinergic signalling in neocortical neurons. J Neurophysiol. 2007; 97(3):2215–2229. [PubMed: 17122323]

Hasselmo ME, Bower JM. Cholinergic suppression specific to intrinsic not afferent fiber synapses in rat piriform (olfactory) cortex. J Neurophysiol. 1992; 67(5):1222–1229. [PubMed: 1597708]

Hasselmo ME, McGaughy J. High acetylcholine levels set circuit dynamics for attention and encoding and low acetylcholine levels set dynamics for consolidation. Progress in brain research. 2004; 145:207–231. [PubMed: 14650918]

Herrero JL, Roberts MJ, Delicato LS, Gieselmann MA, Dayan P, Thiele A. Acetylcholine contributes through muscarinic receptors to attentional modulation in V1. Nature. 2008; 454(7208):1110–1114. [PubMed: 18633352]

Himmelheber AM, Sarter M, Bruno JP. Increases in cortical acetylcholine release during sustained attention performance in rats. Brain Res Cogn Brain Res. 2000; 9(3):313–325. [PubMed: 10808142]

Hsieh CY, Cruikshank SJ, Metherate R. Differential modulation of auditory thalamocortical and intracortical synaptic transmission by cholinergic agonist. Brain Research. 2000; 880(1–2):51–64. [PubMed: 11032989]

Katzner S, Busse L, Carandini M. GABAA Inhibition Controls Response Gain in Visual Cortex. J Neurosci. 2011; 31(16):5931–5941. [PubMed: 21508218]

Kawaguchi Y. Selective cholinergic modulation of cortical GABAergic cell subtypes. J Neurophysiol. 1997; 78(3):1743–1747. [PubMed: 9310461]

Kawaguchi Y, Kubota Y. Correlation of physiological subgroupings of nonpyramidal cells with parvalbumin- and calbindinD28k-immunoreactive neurons in layer V of rat frontal cortex. J Neurophysiol. 1993; 70(1):387–396. [PubMed: 8395585]

Kimura F. Cholinergic modulation of cortical function: a hypothetical role in shifting the dynamics in cortical network. Neurosci Res. 2000; 38(1):19–26. [PubMed: 10997574]

Kruglikov I, Rudy B. Perisomatic GABA release and thalamocortical integration onto neocortical excitatory cells are regulated by neuromodulators. Neuron. 2008; 58(6):911–924. [PubMed: 18579081]

Markram H, Toledo-Rodriguez M, Wang Y, Gupta A, Silberberg G, Wu C. Interneurons of the neocortical inhibitory system. Nat Rev Neurosci. 2004; 5(10):793–807. [PubMed: 15378039]

McConnell SK, LeVay S. Anatomical organization of the visual system of the mink, Mustela vison. J Comp Neurol. 1986; 250(1):109–132. [PubMed: 3016036]

McCormick DA, Prince DA. Mechanisms of action of acetylcholine in the guinea-pig cerebral cortex in vitro. J Physiol. 1986; 375:169–194. [PubMed: 2879035]

McGaughy J, Sarter M. Sustained attention performance in rats with intracortical infusions of 192 IgG-saporin-induced cortical cholinergic deafferentation: effects of physostigmine and FG 7142. Behav Neurosci. 1998; 112(6):1519–1525. [PubMed: 9926833]

Muir JL, Everitt BJ, Robbins TW. AMPA-induced excitotoxic lesions of the basal forebrain: a significant role for the cortical cholinergic system in attentional function. J Neurosci. 1994; 14(4): 2313–2326. [PubMed: 7512637]

Paxinos, G.; Franklin, KBJ. The mouse brain in stereotaxic coordinates. 2. Academic Press; 2003.

Paxinos, G.; Huang, XF.; Toga, AW. The rhesus monkey brain in stereotaxic coordinates. Academic Press; 2000.

Paxinos, G.; Watson, C. The Rat Brain in Stereotaxic Coordinates. 6. Academic Press; 2007.

Sarter M, Hasselmo ME, Bruno JP, Givens B. Unraveling the attentional functions of cortical cholinergic inputs: interactions between signal-driven and cognitive modulation of signal detection. Brain Res Brain Res Rev. 2005; 48(1):98–111. [PubMed: 15708630]

Schwaller B, Dick J, Dhoot G, Carroll S, Vrbova G, Nicotera P, Pette D, Wyss A, Bluethmann H, Hunziker W, Celio MR. Prolonged contraction-relaxation cycle of fast-twitch muscles in parvalbumin knockout mice. Am J Physiol. 1999; 276(2 Pt 1):C395–403. [PubMed: 9950767]

Turrini P, Casu MA, Wong TP, De Koninck Y, Ribeiro-da-Silva A, Cuello AC. Cholinergic nerve terminals establish classical synapses in the rat cerebral cortex: synaptic pattern and age-related atrophy. Neuroscience. 2001; 105(2):277–285. [PubMed: 11672595]

Umbriaco D, Watkins KC, Descarries L, Cozzari C, Hartman BK. Ultrastructural and morphometric features of the acetylcholine innervation in adult rat parietal cortex: an electron microscopic study in serial sections. J Comp Neurol. 1994; 348(3):351–373. [PubMed: 7844253]

Van Brederode JF, Mulligan KA, Hendrickson AE. Calcium-binding proteins as markers for subpopulations of GABAergic neurons in monkey striate cortex. J Comp Neurol. 1990; 298(1):1–22. [PubMed: 2170466]

White LE, Bosking WH, Williams SM, Fitzpatrick D. Maps of central visual space in ferret V1 and V2 lack matching inputs from the two eyes. J Neurosci. 1999; 19(16):7089–7099. [PubMed: 10436063]

Wong-Riley M, Anderson B, Liebl W, Huang Z. Neurochemical organization of the macaque striate cortex: correlation of cytochrome oxidase with Na+K+ATPase, NADPH-diaphorase, nitric oxide synthase, and N-methyl-D-aspartate receptor subunit 1. Neuroscience. 1998; 83(4):1025–1045. [PubMed: 9502244]

Xiang Z, Huguenard JR, Prince DA. Cholinergic switching within neocortical inhibitory networks. Science. 1998; 281(5379):985–988. [PubMed: 9703513]

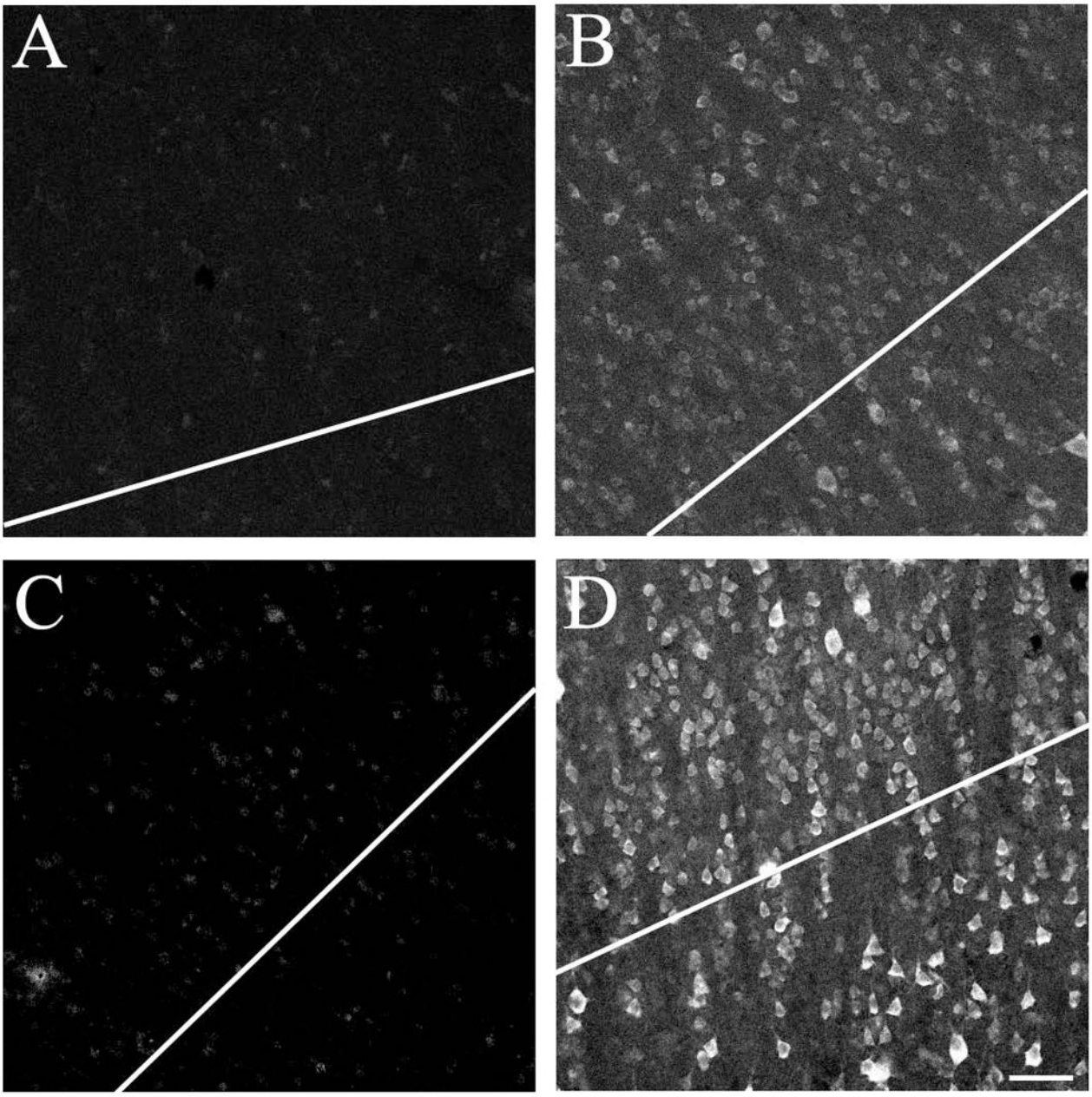

Figure 1.

Water bath antigen retrieval increases number of identifiable immunoreactive neurons per unit area in human tissue. The photomicrographs in Panels **B and D** shows staining for the m1 AChR in tissue from human area V1. In Panel B, the tissue has not undergone heat-based antigen retrieval. The photomicrograph in Panel **D** shows staining for the m1 AChR in tissue that was exposed to 1mM EDTA and one 30-minute incubation in a 80–95°C water bath prior to antibody processing. Immunoreactive neurons are much easier to identify following this treatment. Panels **A** and **C** show tissue processed with a preadsorbed m1 AChR antibody, in untreated (**A**) and heat treated (**C**) tissue. In each case the tissue used for preadsorption was from the same section as that processed with the regular antibody, i.e. the section was cut in half prior to being placed in primary antibody (and therefore after heat

treatment in Panels **C** and **D**). All images are of layer 4c; note that antigen retrieval does not noticeably increase the appearance of layer 4c neuropil staining. Antibody dilution for all panels 1:1000. Scale bar = 50μm.

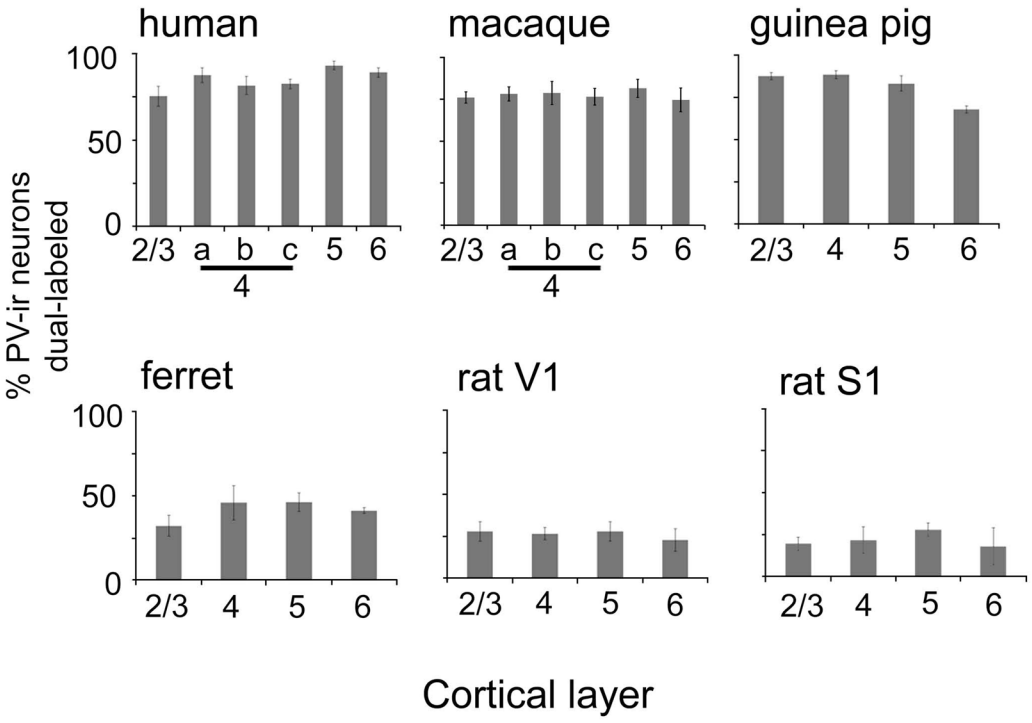

Figure 2.

Quantification of dual immunoreactivity for parvalbumin and m1 AChRs. Each plot shows, by species (separate plots) and cortical layer (x axis) the percentage of PV-ir neurons encountered in area V1 (area S1 in the far right plot) that were also immunoreactive for m1 AChRs. It can be seen that in all species there is a flat laminar profile. It can also be seen that more PV-ir neurons in humans, macaques and guinea pigs express m1 receptors than do PV-ir neurons in ferrets or rats. Error bars represent SEM. Number of PV-ir neurons in each graph: human=845, macaque=326, guinea pig=355, ferret=203, rat V1=366, rat S1=233.

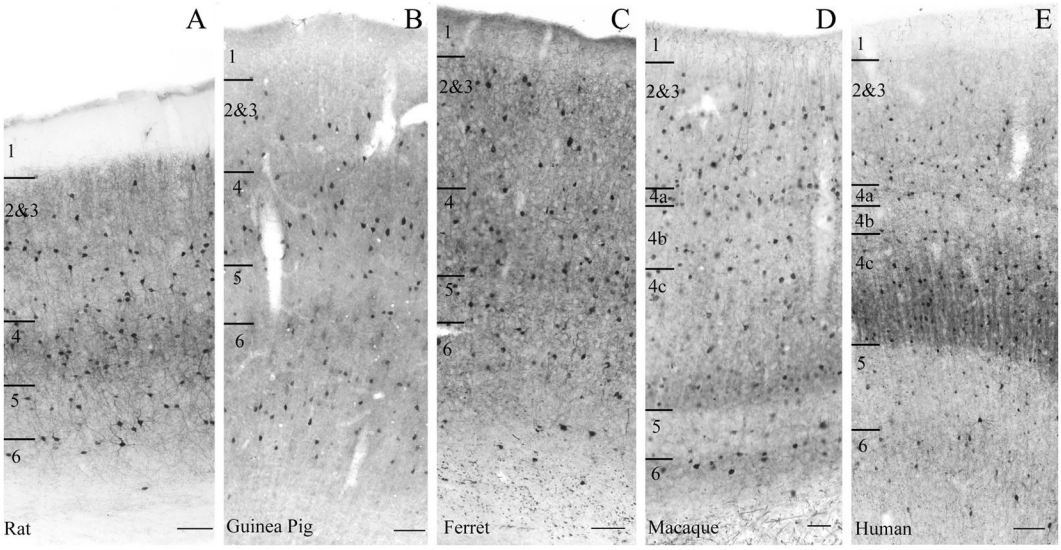

Figure 3.

Qualitative comparison of immunoreactivity for parvalbumin in V1 of the rat (**A**), guinea pig (**B**), ferret (**C**), macaque (**D**), and human (tissue processed without antigen retrieval, **E**). It can be seen that in each species parvalbumin-immunoreactive neurons are present in all cortical layers (there some in layer 1 as well, not shown here but see Fig. 4). There is denser staining of the neuropil and an apparently higher density of somata in the thalamic recipient layers (layers 4 & 6 in rat, guinea pig and ferret; layers 4a, 4c and 6 in macaque and human). The immunoreactive band in layer 4c of the human is particularly striking. Also evident is the fainter, more diffuse nature of the neuropil staining in the guinea pig, compared with all of the other species. Layer boundaries are indicated on the left of each panel. Scale bars = 100μm.

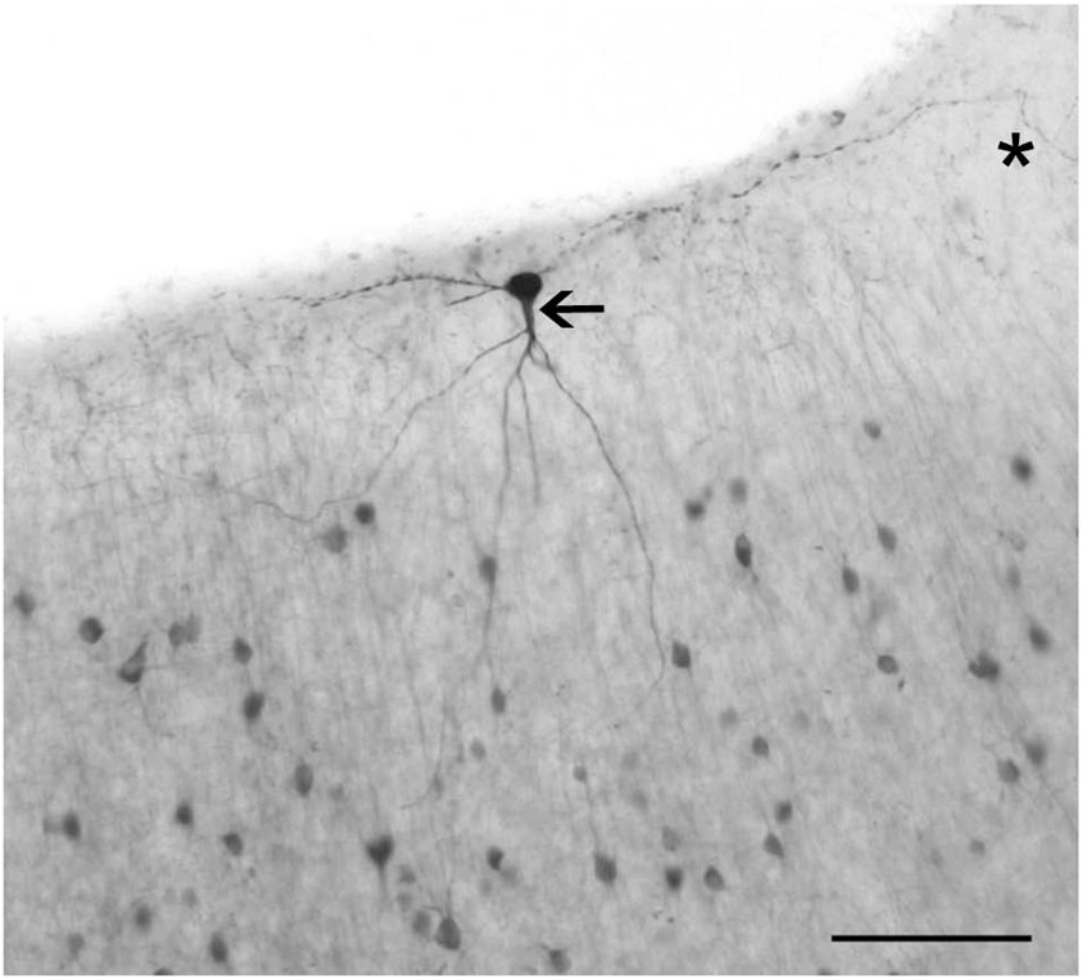

Figure 4.

A large, parvalbumin-immunoreactive neuron in layer 1 of macaque V1. While parvalbumin neurons are rare in layer 1, they are present. Here we show a large neuron of a roughly "inverted pyramidal" morphology with its soma in layer 1. The cell's axon extends laterally through layer 1 on both sides of the soma, before turning down toward layer to the right of the picture, although it appears a branch may continue along in layer 1 (*). Emerging from the soma is one prominent dendrite (arrow) reaching down and branching into layer 2 and across the layer1/2 border. There is a secondary dendrite emerging and immediately branching to the left of the soma, it appears to remain in layer 1. Scale bar = 100μm.

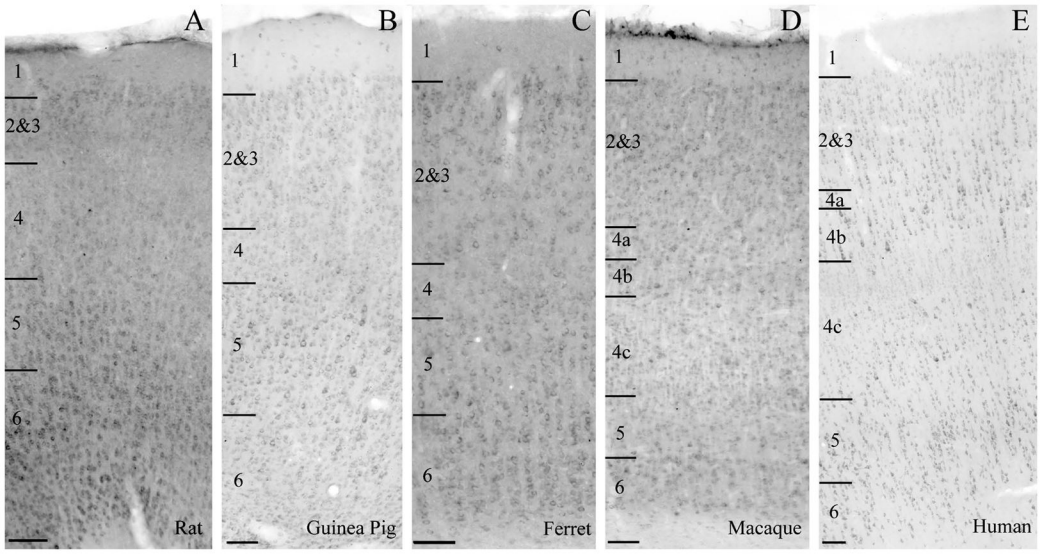

Figure 5.

Qualitative comparison of immunoreactivity for m1 muscarinic acetylcholine receptors in V1 of the rat (**A**), guinea pig (**B**), ferret (**C**), macaque (**D**), and human (**E**). Immunoreactivity for the m1 ACh receptor in all species is characterized by a cytoplasmic ring within the cell body. The intensity of neuropil staining varies between species. In guinea pigs (**B**), macaques (**D**) and humans (**E**), neuropil staining is generally weaker and somatic staining appears intense. In rats (**A**) and ferrets (**C**) there is diffuse staining of the neuropil in all layers leading to an overall darker appearance of the tissue. Note the large, strongly m1-immunoreactive somata in layer 4b, which are particularly apparent in the micrograph taken of human V1. Layer boundaries are indicated on the left of each panel. Scale bars = 100μm.

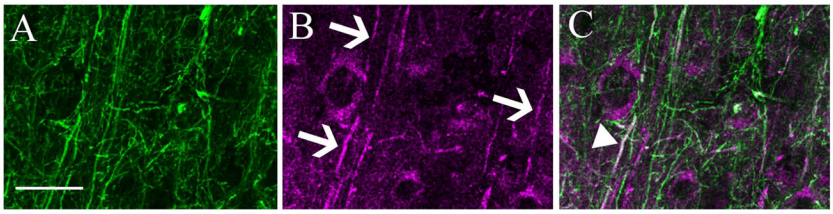

Figure 6.

Dual labeling for m1 ACh receptors and parvalbumin in layer 5 of ferret V1. Panel **A** shows the isolated immunoreactivity for parvalbumin. A dense plexus of axons and dendrites is evident. Panel **B** shows isolated immunoreactivity for the m1 ACh receptor. A number of labeled dendrites are visible (arrows). In the merged image (**C**), there is one dendrite that is clearly immunoreactive for both m1 AChRs and for PV (arrowhead), this dually-labeled process appears white in the combined channel image. In this case, because there is a length of dendrite showing immunoreactivity in both channels, the possibility of a false positive is very low – this is very likely to be the dendrite of the PV neuron containing m1 receptors. There are other dendrites in this panel, which appear purely green, and are m1 immunoreactive dendrites that may or may not belong to PV neurons. Scale bar = 50μm.

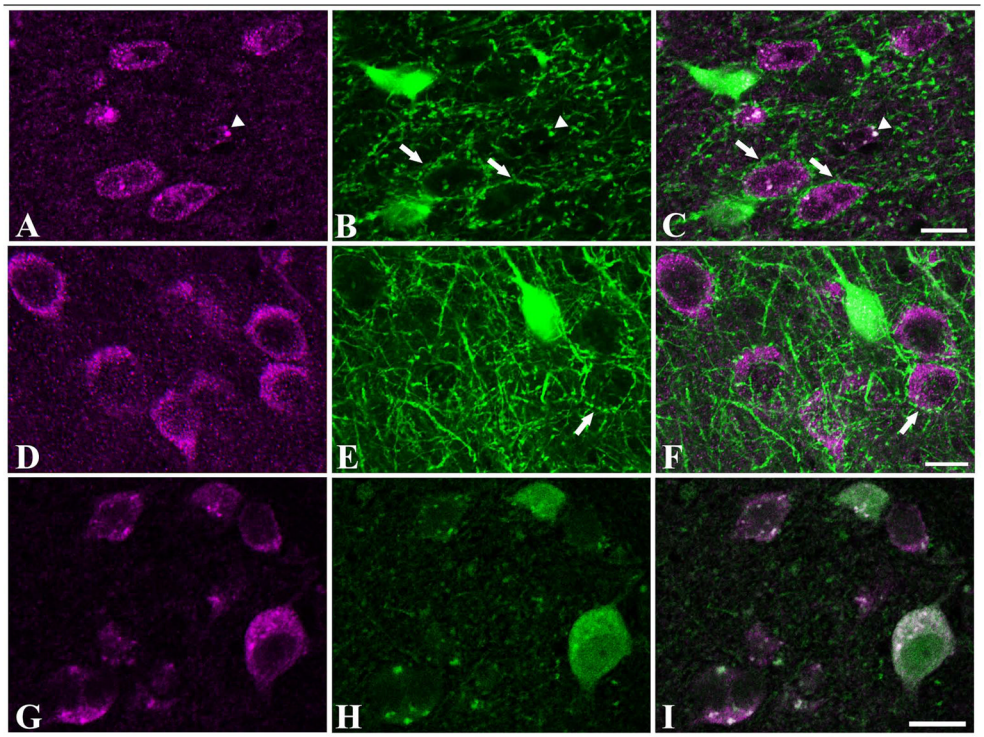

Figure 7.

Parvalbumin immunoreactive perisomatic baskets are not immunoreactive for m1 ACh receptors. In these images from layer 3 of rat (A–C) and ferret (D–F) V1, a number of varicose, parvalbumin-immunoreactive perisomatic baskets are visible (for example, wide arrows in B, C, E, and F). The cell bodies inside the baskets are often m1-immunoreactive (*s in panels A, C, D, and F). In general, the varicosities that make up these baskets are not immunoreactive for m1 ACh receptors. The two strongly fluorescent points in figures A–C (arrowhead) may be dually-immunoreactive boutons, but they do not appear to be part of a basket. In fact their large size, lack of a connecting axon and the striking intensity of the fluorescence in the magenta channel (A) suggest that they may be non-specific autofluorescence. While the staining of human V1 (G–I) was good enough to allow counting of cell bodies, neuropil immunoreactivity was not well-preserved in these samples to assess whether parvalbumin-immunoreactive boutons express m1 ACh receptors in human V1. Scale bars = 10μm.

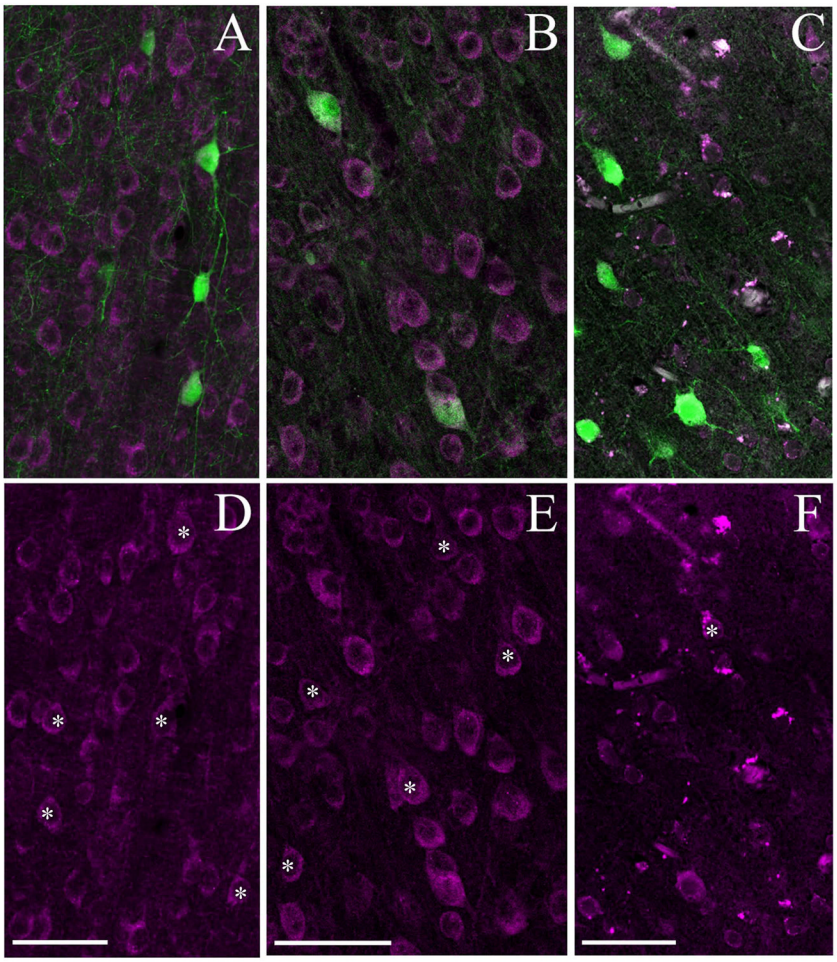

Figure 8.

m1 ACh receptor immunoreactivity in parvalbumin-immunonegative neurons is common in non-primate species. Panels **A–C** show dual immunoreactivity for parvalbumin (green) and m1 AChRs (magenta) in ferret (**A**), guinea pig (**B**) and human (**C**) V1. It can be seen that many neurons in ferret and guinea pig V1 are singly labeled for m1 ACh receptors while there appear to be fewer singly labeled m1-immunoreactive neurons in human V1 (**C**). In the isolated channel showing m1 ACh receptor immunoreactivity (Panels **D–E**) there is the appearance of a denser packing of m1 immunoreactive neurons in ferret (**D**) and guinea pig (**E**) than in human (**F**) and the cell bodies in panels **D** and **E** also appear larger and more often have a “pyramidal” appearance (example “pyramidal-like” somata marked by *). Scale bars = 50μm.

Table 1

Species used, tissue sources and fixation conditions

Species	N	Source	Perfused by	Exsanguination solution	Fixative
WT mouse	2	Nathanson (U. Washington)	donor	0.9% Saline	4% PFA
KO mouse	2	Nathanson (U. Washington)	donor	0.9% Saline	4% PFA
KO mouse	9	Wess (NIH)	AD	Heparinized PBS	4% PFA
Rat	3	Callaway, Chichilnisky (Salk)	AD, donor	Heparinized PBS	4% PFA
Guinea pig	4	Elm Hill	AD	Heparinized PBS	4% PFA
Ferret	3	Callaway (Salk)	AD	Heparinized PBS	4% PFA
Macaque	6	Movshon, Glimcher (NYU), Das, Gottleib (Columbia), Callaway (Salk)	AD	Heparinized PBS	4% PFA

Table 2

Human sample demographics.

ID #	Age	Gender	PMI	Race	Clinical Diagnosis	Pathologic Diagnosis	Raw # PV neurons	Raw % dual label
6089	51	M	4	C	NC-EtOH cirrhosis	NC (0, 0, N/A)	167	89%
6077	64	F	6	AA	NC-met lung CA	AD-aging (B, II, low)	202	81%
6201	64	M	10	C	NC-gastric CA	NC (0, 0, N/A)	181	79%
6145	43	F	10	C	NC-lumbar ependymoma	NC (0, 0, N/A)	43	77%
6064	48	M	12	unk	NC-CA, unk primary	NC (0, 0, N/A)	252	81%

PMI: post-mortem interval.

Table 3

Primary antibodies.

Antigen	Immunogen
m1 muscarinic acetylcholine receptor	GST fusion protein corresponding to aa227–353 of human m1 ACh Receptor (GSETPGKGGGSSSSSERSQPGAEGSPETPPGRCCRCCRAPRLLQAYSWKEEEEEDEGSMESLTSSEGEEPGESVVIKMPMVDPEAQAPTKQPPRSSPNT
parvalbumin	Purified carp parvalbumin

Table 4

Mean soma size (in μm) by cell-type for each species.

	Rat V1	Rat S1	Guinea pig	Ferret	Macaque	Human
PV-ir	15.68(3.59)	16.99(2.44)	16.95(2.87)	17.04(5.33)	13.23(2.22)	15.36(2.74)
m1-ir	16.55(2.30)	16.74(2.84)	17.18(4.51)	18.59(4.54)	13.68(3.93)	16.12(4.47)

Values in parentheses are the standard deviation of the mean. N for each cell is 10 neurons.

Table 5

Percentage of PV-ir neurons that were also immunoreactive for m1 AChRs, V1 comparison by species. “Corrected” counts refer to the Abercrombie correction (See Methods).

	Raw N PV	Corrected N PV	Raw N m1	Corrected N m1	% dual label
Rat	366	256.2	1539	1067.91	27% (sd 11.1)
Guinea pig	355	237.85	2254	1487.64	85% (sd 5.0)
Ferret	203	133.98	1137	727.68	41% (sd 14.5)
Macaque	557	406.61	4465	3214.8	76% (sd 5.1)
Human	845	566.15	3757	2479.62	81% (sd 4.7)

Percentages are calculated as a mean across animals within each species, reported standard deviations for this comparison across individuals. N (animals) =3 (rat), 4 (guinea pig), 3 (ferret), 6 (macaque), and 5 (human).